CHEMISTRY OF MATERIALS

Article

pubs.acs.org/cm

Influence of Alkyl Side Chain on the Crystallinity and Trap Density of States in Thiophene and Thiazole Semiconducting Copolymer Based Inkjet-Printed Field-Effect Transistors

Jiyoul Lee,[†,‡] Jong Won Chung,[†,‡] Jaeman Jang,[#] Do Hwan Kim,[§] Jeong-Il Park,[†] Eunkyung Lee,[†] Bang-Lin Lee,*[,†] Joo-Young Kim,[†] Ji Young Jung,[†] Joon Seok Park,[†] Bonwon Koo,[†] Yong Wan Jin,[†] and Dae Hwan Kim*[,#]

[†]Materials R&D Center, Samsung Advanced Institute of Technology, San #14, Nongseo-dong, Giheung-gu, Yongin-si, Gyeonggi-do, 446-712, Korea

[#]School of Electrical Engineering, Kookmin University, Jeongneung-dong, Seongbuk-gu, Seoul, 136-702, Korea

[§]Department of Organic Materials and Fiber Engineering, Soongsil University, Sangdoro 369, Dongjak-gu, Seoul, 156-743, Korea

Supporting Information

ABSTRACT: The influence of alkyl side chains on the crystallinity of semiconducting copolymer films and their sub-bandgap density-of-states (DOS), the latter being closely related to the stability and the device performance of organic field-effect transistors (OFETs), is investigated. Three different poly(hexathiophene-alt-bithiazole) (PHTBTz) based polymer semiconductors, with identical backbones but different side chain positions and lengths, were synthesized. The crystallinity examined by grazing incidence X-ray diffraction (GIXRD) strongly depends on the number, position, and length of each type of alkyl side chain attached to the thiophene and thiazole copolymer backbones. Also, the sub-bandgap trap DOS distributions were extracted by performing multiple-frequency capacitance−voltage (MF-CV) spectroscopy on the field effect devices. The relationship between film crystallinity and trap DOS in the field-effect transistors can be interpreted in terms of the complex interplay between the number, position, and length of each alkyl side chain for efficient $\pi-\pi$ stacking. In particular, the number and position of the alkyl side chain attached to the polymer backbone significantly affects the device performance. Poly(tetryloctylhexathiophene-alt-dioctylbithiazole) (PHTBTz-C8) exhibits the best electrical performance among the different semiconductors synthesized, with a relatively low bulk trap density of ~2.0×10^{20} cm^{-3} eV^{-1} as well as reasonable hole mobility of ~0.25 cm^2 V^{-1} s^{-1}. The microstructural analyses of this organic material strongly suggest that the short $\pi-\pi$ stacking distance induces strong interaction between adjacent polymer backbones, which in turn results in enhanced electrical properties.

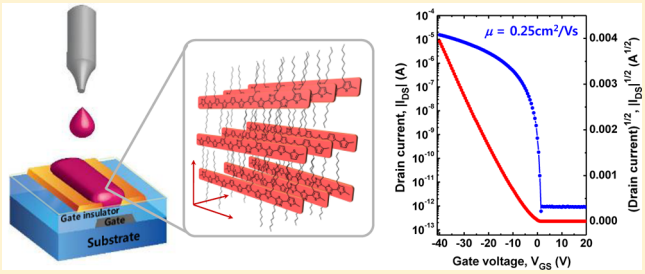

KEYWORDS: *polymer semiconductor, field-effect transistors, inkjet-printing, X-ray diffraction, density of states*

INTRODUCTION

Printed electronics, the art of printing the electrical devices directly on various substrates, has attracted a lot of interest with regards to potential feasibility of high throughput, continuous, and efficient deposition of materials onto flexible substrates. For the implementation of printed electronics, a variety of functional inks based on metallic, semiconducting, and insulating materials have been developed, and various methods have been demonstrated to fabricate printed electronic components onto flexible substrates.[1,2] However, the design and synthesis of novel substances with good printability that result in enhanced device performance are still important and challenging issues in the field. Several research groups have conducted intensive research in order to develop such materials, and accordingly a variety of conjugated organic materials have been suggested for potential use as active semiconductors in printed devices.[3−5]

Organic semiconductors can be classified into two categories: oligomers (or small-molecules) and polymers (or macromolecules). Both kinds have their own advantages in terms of processability and device performance.[6,7] Oligomer thin films usually exhibit highly ordered microstructures, which is beneficial for the efficient transport of charge carriers, and thus high carrier mobility can be achieved in the corresponding organic field-effect transistors (OFETs). However, the highly ordered microstructure in the small-molecule organic films inevitably results in directional or anisotropic charge transport, which may be detrimental with regards to areal uniformity for large-area applications. On the other hand, polymer semiconductors inherently have dispersions along the polymer chain

Received: February 20, 2013
Revised: April 8, 2013
Published: April 9, 2013

dx.doi.org/10.1021/cm400592b | *Chem. Mater.* 2013, 25, 1927−1934

Scheme 1. Synthesis Routes of PHTBTz Semiconducting Copolymer Series

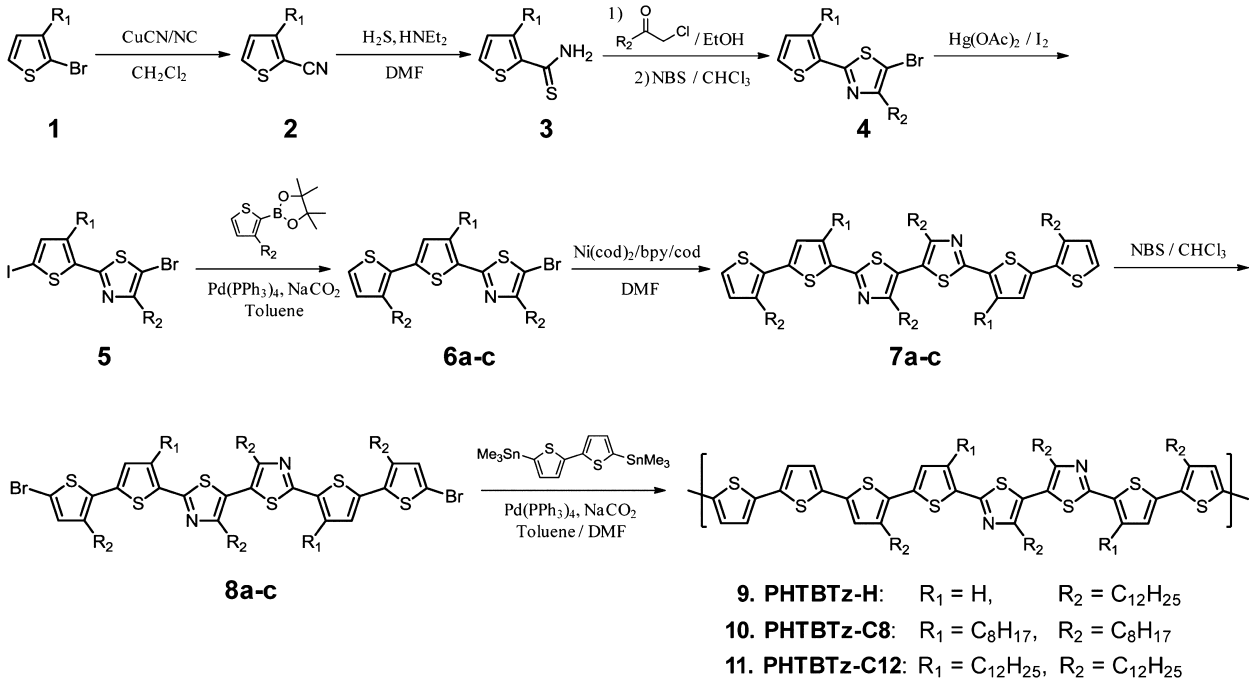

length, which suppresses self-organization during film-formation, leading to relatively loose $\pi-\pi$ packing and lower carrier mobility in comparison with small-molecules. Yet, polymer semiconductors typically exhibit even morphologies with minimal grain boundaries and have an excellent film-forming nature, which is critical for the realization of uniform large-area electronics by the printing technique.[8]

Generally, in order to use organic semiconductors including oligomers and polymers as the printing ink, sufficiently good solubility of semiconducting materials in organic solvents is necessary, and this requires the presence of appropriate functional groups (e.g., long and/or branched alkanes), attached to their main backbone. In particular, the performance of polymer semiconductors as active layers in field-effect transistors strongly depends on the number, position, and length of the alkyl side chain attached to its main backbone. Thus, the investigation on the effect of various functional side chains on the crystallinity and trap density of states (DOS) of semiconducting polymers in OFETs is very important in order to offer a guideline to design and synthesize high performance semiconducting polymers.

In the present work, we have prepared three thiophene/thiazole based semiconducting copolymers - poly (didodeocylhexathiophene-alt-didodecylbithiazole) (PHTBTz-H), poly-(tetryloctylhexathiophene-alt-dioctylbithiazole) (PHTBTz-C8), and poly(tetryldodecyl-hexathiophene-alt-didodecylbithiazole) (PHTBTz-C12), where the thiophene acts as an electron-donating unit and the thiazole is the electron-accepting part. The presence of thiazole units within the molecular backbone is anticipated to stabilize the highest occupied molecular orbital (HOMO) level, planarize the molecules, and thus enhance the intramolecular charge transfer leading to high charge carrier mobility.[9−13] Here, the PHTBTz series with identical backbones but different side chain positions and lengths is examined, and the influence of the alkyl side chain attached to the backbone on the crystallinity of the films, the sub-bandgap DOS, and the device performance such as field-effect mobility in OFETs is investigated.

EXPERIMENTAL SECTION

General Considerations. All chemicals were purchased from Aldrich and used without additional purification. The general synthetic routes of the PHTBTz series are shown in Scheme 1. ^{1}H NMR spectra were recorded with Bruker Avance digital 300 (300 MHz) and Bruker Avance III (600 MHz) spectrometers. All NMR spectra were referenced to the solvent. ^{13}C NMR spectra were also collected. Proton (0.1 ppm) chemical shifts were measured with respect to internal TMS in $CDCl_3$. ^{13}C chemical shifts were reported in ppm relative to $CDCl_3$. Column chromatography was performed on Merck silicagel 60. Mass spectra were measured using a Bruker, Ultraflex III TOF/TOF 200 mass spectrometer. UV−visible absorption spectra were recorded with a Varian cary 5000 UV−vis−NIR spectrophotometer using thin-film samples. The melting temperature of the compounds was determined using differential scanning calorimetry (DSC). An atomic force microscope (Digital Instruments Multimode) operating in tapping mode with a silicon cantilever was used to characterize the surface morphologies of the samples. The grazing-incidence X-ray diffraction measurements (GIXRD) were performed at the Stanford Synchrotron Radiation Laboratory on beamlines 11-3. The incident photon energy was 12.7 keV, and the incidence angle was fixed at 0.12 degrees. Vertical slits were 50 μm apart, and horizontal slits were 150 μm apart.

Compounds 1−6a−c. The compounds **1−6a−c** were synthesized according to the method described in our previous publication.[9,10] Yellowish-white powders were obtained with good yield.

Compound 6a. ^{1}H NMR (300 MHz, $CDCl_3$, δ): 7.33 (d, J = 3.8 Hz, 1H), 7.20 (d, J = 5.2 Hz, 1H), 7.05 (d, J = 3.9 Hz, 1H), 6.94 (d, J = 5.2 Hz, 1H), 2.79 (t, J = 7.8 Hz, 2H), 2.73 (t, J = 7.6 Hz, 2H), 1.72−1.62 (m, 4H), 1.33−1.25 (m, 36H), 0.90−0.83 (m, 6H).

Compound 6b. ^{1}H NMR (300 MHz, $CDCl_3$, δ): 7.20 (d, J = 3.9 Hz, 1H), 6.95 (s, 1H), 6.94 (d, J = 3.9 Hz, 1H), 2.86−2.74 (m, 6H), 1.74−1.63 (m, 6H), 1.43−1.28 (m, 36H), 0.91−0.86 (m, 9H).

Compound 6c. ^{1}H NMR (300 MHz, CDCl3, δ): 7.19 (d, J = 4.8 Hz, 1H), 6.94 (s, 1H), 6.93 (d, J = 4.8 Hz, 1H), 2.86−2.72 (m, 6H), 1.69−1.59 (m, 6H), 1.40−1.25 (m, 54H), 0.90−0.85 (m, 9H).

Compound 7a. In a reactor in a nitrogen atmosphere, a nickel(0) compound ($Ni(cod)_2$, 0.93 g, 3.38 mmol), bipyridine (bpy, 0.53 g,

dx.doi.org/10.1021/cm400592b | Chem. Mater. 2013, 25, 1927−1934

3.38 mmol), and cyclooctadiene (0.53 g, 3.38 mmol) were added to 70 mL of anhydrous dimethyl formamide (DMF), and the mixture was stirred at 60 °C for about 30 min. The compound **6a** (3.0 g, 4.51 mmol) was then added to the reaction mixture, which was then stirred at 90 °C for 48 h. After the reaction, a mixture solution of ammonium hydroxide and methanol (mixing ratio = 1:2, about 1.2 L) was added to the reaction solution and stirred for about 12 h. Subsequently, the product solid obtained by filtering was dissolved in chloroform and then reprecipitated several times in methanol. After drying for about 24 h in vacuum, a compound was obtained; **7a** (yield = 94.3%). ^{1}H NMR (300 MHz, $CDCl_3$, δ): 7.44 (d, J = 3.9 Hz, 2H), 7.22 (d, J = 5.2 Hz, 2H), 7.11 (d, J = 3.9 Hz, 2H), 6.96 (d, J = 5.2 Hz, 2H), 2.82 (t, J = 7.7 Hz, 4H), 2.68 (t, J = 7.7 Hz, 4H), 1.72−1.61 (m, 8H), 1.26−1.23 (m, 72H), 0.90−0.84 (m, 12H).

Compound 7b. This compound was obtained according to the procedure described above for **7a**. ^{1}H NMR (300 MHz, $CDCl_3$, δ): 7.20 (d, J = 5.4 Hz, 2H), 6.98 (s, 2H), 6.95 (d, J = 5.4 Hz, 2H), 2.81 (t, J = 7.8 Hz, 4H), 2.70 (t, J = 7.8 Hz, 4H), 1.73−1.61 (m, 12H), 1.44−1.27 (m, 60H), 0.89−0.83 (m, 18H).

Compound 7c. This compound was obtained according to the procedure described above for **7a** ^{1}H NMR (300 MHz, $CDCl_3$, δ): 7.19 (d, J = 5.4 Hz, 2H), 6.98 (s, 2H), 6.95 (d, J = 5.1 Hz, 2H), 2.91 (t, J = 7.7 Hz, 4H), 2.82 (t, J = 7.8 Hz, 4H), 2.70 (t, J = 7.7 Hz, 4H), 1.73−1.64 (m, 12H), 1.41−1.23 (m, 108H), 0.87−0.84 (m, 18H).

Compound 8a. The obtained compound **7a** (2.49g, 2.13 mmol) was reacted with NBS (0.79 g, 4.46 mmol) in a chloroform solution (120 mL) with acetic acid. The mixture was stirred at room temperature overnight. The solvent was removed by heating under vacuum, and the residue was dissolved in chloroform and washed with brine. The collected organic layer was dried over sodium sulfate, and the organic solvent was removed by rotary evaporation. The residue was purified by silica column purification (n-hexane:chloroform = 5:1), and the collected compound was purified by recrystallization in ethanol to yield **8a** as a reddish-orange powder in yield = 84.0%. ^{1}H NMR (300 MHz, $CDCl_3$, δ): 7.42 (d, J = 3.9 Hz, 2H), 7.02 (d, J = 3.9 Hz, 2H), 6.92 (s, 2H), 2.75 (t, J = 7.7 Hz, 4H), 2.68 (t, J = 7.6 Hz, 4H), 1.73−1.60 (m, 8H), 1.25−1.23 (m, 72H), 0.90−0.84 (m, 12H); ^{13}C NMR (125 MHz, $CDCl_3$, δ): 159.82, 148.83, 141.06, 137.42, 136.85, 134.30, 132.83, 131.49, 129.66, 126.71, 126.39, 119.23, 111.27, 91.08, 38.05, 31.92, 29.67, 29.64, 29.55, 29.42, 29.37, 22.69, 14.13; MALDI TOF MS: 1326.50 [M+H]; calculated exact mass: 1326.65; Elemental Analysis: calculated for $C_{70}H_{106}Br_2N_2S_6$: C, 63.32; H, 8.05; N, 2.11; S, 14.49. found: C, 63.00; H, 7.70; N, 1.91; S, 15.01.

Compound 8b. This compound was obtained according to the procedure described above for **8a**. ^{1}H NMR (300 MHz, $CDCl_3$, δ): 6.91 (d, J = 2.1 Hz, 4H), 2.89 (t, J = 7.8 Hz, 4H), 2.75 (t, J = 7.8 Hz, 4H), 2.69 (t, J = 7.8 Hz, 4H), 1.74−1.60 (m, 12H), 1.43−1.27 (m, 60H), 0.89−0.83 (m, 18H); ^{13}C NMR (125 MHz, $CDCl_3$, δ): 159.67, 156.90, 142.71, 140.87, 135.65, 132.83, 131.76, 129.28, 119.42, 110.97, 31.87, 30.43, 30.09, 29.83, 29.73, 29.65, 29.47, 29.43, 29.38, 29.28, 29.23, 22.67, 14.10; MALDI TOF MS: 1326.50 [M+H]; calculated exact mass: 1326.66; Elemental Analysis: calculated for $C_{70}H_{106}Br_2N_2S_6$: C, 63.32; H, 8.05; N, 2.11; S, 14.49. found: C, 63.49; H, 7.83; N, 2.03; S, 14.26.

Compound 8c. This compound was obtained according to the procedure described above for **8a**. ^{1}H NMR (300 MHz, $CDCl_3$, δ): 6.91 (d, J = 1.8 Hz, 4H), 2.89 (t, J = 7.8 Hz, 4H), 2.75 (t, J = 7.8 Hz, 4H), 2.69 (t, J = 7.8 Hz, 4H), 1.73−1.60 (m, 12H), 1.43−1.23 (m, 108H), 0.89−0.83 (m, 18H); ^{13}C NMR (125 MHz, $CDCl_3$, δ): 159.69, 156.92, 142.75, 140.90, 135.74, 132.84, 131.81, 131.51, 129.29, 119.45, 111.00, 31.93, 30.44, 30.11, 29.66, 29.49, 29.37, 22.69, 14.10; MALDI TOF MS: 1663.38 [M+H]; calculated exact mass: 1660.88; Elemental Analysis: calculated for $C_{94}H_{154}Br_2N_2S_6$: C, 67.83; H, 9.33; N, 1.68; S, 11.56. found: C, 67.85; H, 9.08; N, 1.59; S, 11.20.

Compound 9. (PHTBTz-H): 2,5-Bis(trimethylstannyl)thiophene (0.13 g, 0.26 mmol) and compound **8a** (0.4 g, 0.38 mmol) were dissolved in a mixture of anhydrous DMF/THF in a N_2 atmosphere. Subsequently, $Pd(PPh_3)_4$ (43.0 mg, 10 mol %) was added to the mixture and reacted at 85 °C for 60 min, and then the mixture was stirred for 2 h after the addition of an excess amount (1.41 g, 3.76 mmol) of 2-tributylstannylthiophene as an end-capper. The polymer was poured into 300 mL of dilute aqueous HCl/MeOH (1/2) solution and then filtered to produce a dark reddish solid. The obtained polymer solid was dissolved in $CHCl_3$ and was washed with a dilute aqueous HCl solution, NH_4OH (aq), and distilled water sequentially. The crude polymer was precipitated into MeOH and was fractionated by Soxhlet extraction with methanol, acetone, dichloromethane, and chloroform. The chloroform fraction was characterized and used. Removal of the chloroform solvent was followed by drying for 2 days in vacuum and yielded a dark red solid (0.23 g, yield = 53%). GPC (100 °C in trichlorobenzene, polystyrene standards): Mn = 16,289, PDI = 2.07; ^{1}H NMR (300 MHz, $CDCl_3$, δ): 7.09 (m, thiophene-H), 7.02 (m, thiophene-H), 6.90 (m, thiophene-H), 2.92 (broad, alkyl-H), 2.81 (broad, alkyl-H), 2.71 (broad, alkyl-H), 1.72 (broad, alkyl-H), 1.26 (broad, alkyl-H), 0.87 (m, methyl-H); Elemental Analysis: calculated for C78H112N2S8: C, 70.21; H, 8.46; N, 2.10; S, 19.23. found: C, 70.28; H, 8.19; N, 1.99; S, 19.11; UV−vis spectrum: λ_{max} = 490 nm (solution, in $CHCl_3$), λ_{max} = 513 nm (film state from chlorobenzene solution).

Compound 10. (PHTBTz-C8): The same procedure as for **9** was applied for this synthesis, starting with a mixture of compound **8b** (0.60 g, 2.40 mmol) and 2,5-Bis(trimethylstannyl)thiophene (0.79 g, 2.40 mmol). GPC (100 °C in trichlorobenzene, polystyrene standards): Mn = 14,204, PDI = 2.14; ^{1}H NMR (300 MHz, $CDCl_3$, δ): 7.09 (s, Ar−H), 7.02 (d, Ar−H), 2.92 (broad, alkyl-H), 2.82 (broad, alkyl-H), 2.71 (broad, alkyl-H), 1.75 (broad, alkyl-H), 1.43−1.24 (broad, alkyl-H), 0.88−0.84 (m, methyl-H); Elemental Analysis: calculated for $C_{78}H_{112}N_2S_8$: C, 70.21; H, 8.46; N, 2.10; S, 19.23. found: C, 70.19; H, 7.98; N, 2.01; S, 19.98; UV−vis spectrum: λ_{max} = 475 nm (solution, in $CHCl_3$), λ_{max} = 540 and 586 nm (film state from chlorobenzene solution).

Compound 11. (PHTBTz-C12): The same procedure as for **9** was applied for this synthesis, starting with a mixture of compound **8c** (0.6 g, 2.40 mmol) and 2,5-Bis(trimethylstannyl)thiophene (0.789 g, 2.40 mmol). GPC (100 °C in trichlorobenzene, polystyrene standards): Mn = 15,058, PDI = 1.85; ^{1}H NMR (300 MHz, $CDCl_3$, δ): 7.09 (s, Ar−H), 7.02 (d, Ar−H), 2.91 (broad, alkyl-H), 2.82 (broad, alkyl-H), 2.71 (broad, alkyl-H), 1.74−1.61 (broad, alkyl-H), 1.43−1.24 (broad, alkyl-H), 0.89−0.85 (m, methyl-H); Elemental Analysis: calculated for $C_{102}H_{160}N_2S_8$: C, 73.32; H, 9.65; N, 1.68; S, 15.35. found: C, 73.28; H, 9.09; N, 1.60; S, 15.15; UV−vis spectrum: λ_{max} = 474 nm (solution, in CHCl3), λ_{max} = 545 and 590 nm (film state from chlorobenzene solution).

Sample Preparation for Charaterization. In order to confirm the nanomorphology and molecular orientation, PHTBTz-H, -C8, and -C12 thin films were spin-coated using 1 wt % solutions in chlorobenzene on ODTS-treated SiO_2 substrates and annealed at 180 °C, 160 °C, and 140 °C, respectively, for 1 h in a N_2 atmosphere.

Device Fabrication and Electrical Characterization. The electrical properties of PHTBTz series were evaluated using coplanar structured OFETs. The PHTBTz's based OFETs were fabricated using spin-coating and inkjet printing. For the spin-coated film based OFET devices, heavily doped silicon wafers were used, and steel shadow masks were used for the formation of Au source/drain electrode patterns. Then, the polymer thin films were spun from a 1.0 wt % chlorobenzene solution of the polymers. On the other hand, for the fabrication of inkjet-printed OFETs, molybdenum (Mo) was sputter-deposited onto glass substrates as the first step. The deposited Mo was then patterned to form a gate electrode by photolithography. Next, a 300 nm thick silicon dioxide (SiO_2, capacitance C_i = 10 nF cm^{-2}) was deposited by plasma enhanced chemical vapor deposition (PECVD) as the gate dielectric. Source-drain electrodes (Au: thickness ~70 nm) were next deposited by e-beam evaporation and patterned again by photolithography, resulting in a channel width of 120 μm and length of 12 μm. The surface of the gate dielectric was then treated with self-assembled monolayers (SAM) of octadecyltrichlorosilane (ODTS) (purchased from Aldrich). Polymer semiconductors were dissolved in tetrahydronaphthalene (THN) to a concentration of 0.2 wt % and then printed onto the already patterned source-drain electrodes using a Dimatix inkjet printer. Finally, PHTBTz-H, -C8, and

-C12 polymer layers were annealed at 180 °C, 160 °C, and 140 °C, respectively, for 1 h in N_2. The thickness of all polymer films was confirmed by a focused ion beam scanning electron microscope (FIB-SEM) to be approximately 30 nm. A Keithley 4200-SCS semiconductor parameter analyzer and an Agilent 4284A LCR meter were used to measure the current−voltage characteristics and the capacitance−voltage characteristics, respectively. All electrical measurements were performed in air ambient.

RESULTS AND DISCUSSION

Material Properties. The side chains in a given conjugated polymer may not only affect the material's solubility in common solvents but also have a strong influence on its optoelectronic properties.[14] Figure 1a shows the UV−vis absorption spectra of the PHTBTz series in dilute chloroform (~10^{-5} mol·L^{-1}). Among the PHTBTz copolymer series, PHTBTz-H containing the least side chains has a bathochromic shifted absorption wavelength compared to the others. It is worthy to note that the lack of side chains results in higher rigidity relative to PHTBTz-C8 and C12. The alkyl-chain structure in Scheme 1 indicates that the backbone of PHTBTz-H is free of steric hindrance between the unsubstituented thiophene unit (R_1 = H) and the alkyl-substituented thiophene (R_2 = $C_{12}H_{25}$), and the planar conformation is thus easily retained in the solution. However, the absorption peak of PHTBTz-H in the thin film state is only shifted by about 20 nm to a longer wavelength of 510 nm, and the shape of the major peak is not much affected (black line in Figure 1b). This indicates that the PHTBTz-H film did not form the ordered phase, and this may be explained by the presence of the unsubstituented thiophene that induces a relatively large distance, preventing the interdigitation of the intermolecular side chains. In contrast, in the absorption spectra of PHTBTz-C8 and -C12 in solution and thin film states shown in Figure 1(a) and (b), bathochromic shifts of the absorption edges and increased intensities of the shoulder bands are observed. The absorption edge is generally known to exhibit bathochromic shifts when the amount of $\pi-\pi$ stacking increases, enabling neighboring polymer backbones to assemble effectively.[14] Despite the difference in side chain length between PHTBTz-C8 and PHTBTz-C12, they exhibit very similar absorption bands in solution and film states. However, as the length of alkyl chains on the PHTBTz's backbone increases, the relative intensity of the shoulder peak at 590 nm decreases. It is speculated that the magnitude of this shoulder peak is related to the $\pi-\pi$ stacking induced by the intermolecular side chain interdigitation, as reported in other polymers.[4,11,15] For the PHTBTz-C8 films, the shoulder peak around 590 nm is more pronounced, indicating a strong interchain interaction and ordered $\pi-\pi$ stacking in the thin-film state. In general, the side chains participate in the molecular interactions between the neighboring polymer chains and determine the resulting thin-film morphology, which is an essential feature for charge carrier transport.

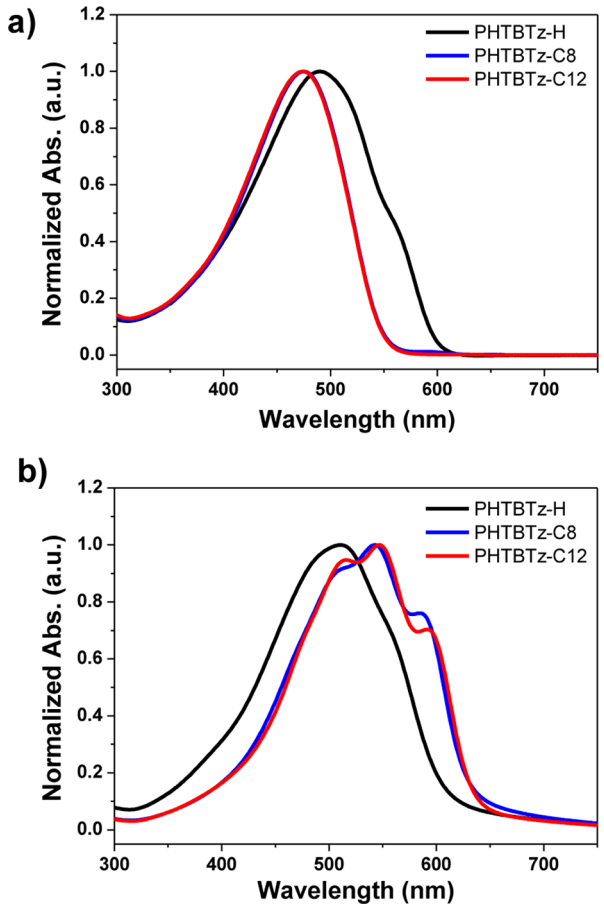

Figure 1. (a) UV−vis absorption spectra of PHTBTz-H (black line), PHTBTz-C8 (blue line), and PHTBTz-C12 (red line) in the chloroform solution. (b) UV−vis absorption spectra of the thin films spin-coated from the chlorobenzene solution, annealed in N_2 for 60 min.

To evaluate the electronic properties of the thin films, the ionization potentials (IPs) were measured. Figure 2 shows the HOMO levels of the spin-coated thin films determined by photoelectron spectroscopy in air (also, listed in Table 1). The IPs of PHTBTz-C8 and -C12 are almost identical (~5.0 eV), whereas that of PHTBTz-H is slightly higher (~5.25 eV), which is attributed to less planar structure of the PHTBTz-H backbone than other polymers in solid state. From the optical band gaps, the LUMO values were calculated to be approximately ~3.22 and ~3.05 eV for PHTBTz-H and PHTBTz-C8/C12, respectively. Thermal analyses of the polymeric semiconductors were also carried out by differential scanning calorimetry (DSC). All polymers were thermally

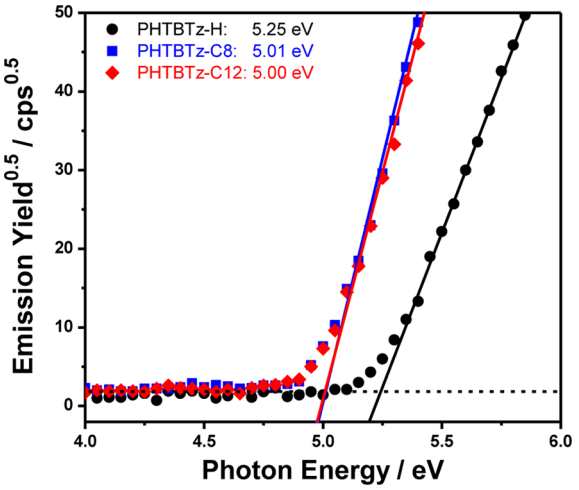

Figure 2. Photoelectron spectroscopy results of the PHTBTz copolymer series in air.

dx.doi.org/10.1021/cm400592b | Chem. Mater. 2013, 25, 1927−1934

Table 1. Chemical and Physical Properties of the PHTBTz Copolymers

polymer	M_n (kg/mol)[a]	PDI[a]	Eg (eV)[b]	IP (eV)[c]	T_m (°C)[d]
PHTBTz-H	16.3	2.07	2.03	5.25	196
PHTBTz-C8	14.2	2.14	1.96	5.01	169
PHTBTz-C12	15.1	1.85	1.95	5.00	102, 144

[a]Determined by high-temperature GPC using the polystyrene standard. [b]Band gaps determined from onsets of absorption peaks of thin films. [c]Evaluated by ambient photoelectron spectroscopy of thin films. [d]Melting temperature determined by DSC.

stable up to 300 °C during the DSC measurements. The transition temperatures are listed in Table 1. Compared to PHTBTz-H and -C8, PHTBTz-C12 exhibited a lower melting temperature, which is consistent with the fact that the increase of the alkyl chain length lowers the melting and crystallization temperature.

Crystallinity and Microstructure of PHTBTz Thin-Films. The crystalline microstructures of the polymer thin films were studied using grazing incidence X-ray diffraction (GIXRD). For the GIXRD measurements, the polymer thin films were prepared by spin-coating a 1.0 wt % chlorobenzene solution of the polymers onto octadecyltrichlorosilane (ODTS) treated SiO_2/p^+-Si wafers, and the films were annealed at an appropriate temperature (180 °C for PHTBTz-H, 160 °C for PHTBTz-C8, and 140 °C for PHTBTz-C12) for 1 h in a N_2 ambient. Figure 3 shows the two-dimensional GIXRD images

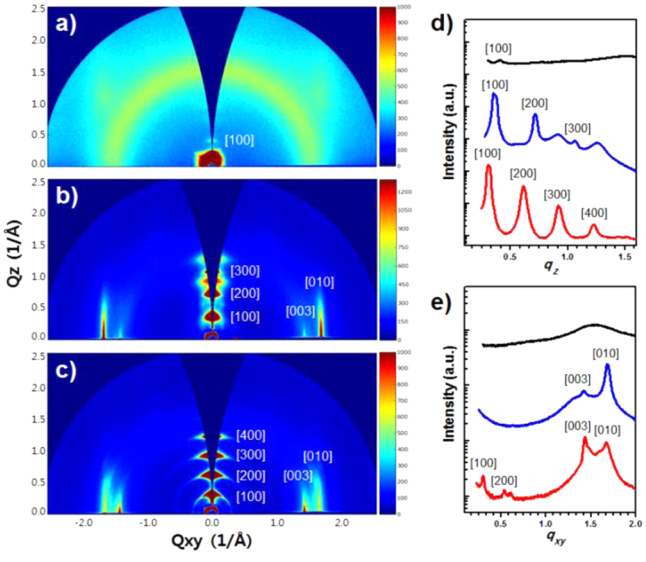

Figure 3. Crystalline microstructure of spin-coated (a) PHTBTz-H, (b) PHTBTz-C8, and (c) PHTBTz-C12 films characterized by 2D-GIXRD. High-resolution (d) specular diffraction patterns (along q_z axis) and (e) grazing incident diffraction patterns (along q_{xy} axis) of the PHTBTz series semiconducting films.

and the GIXRD patterns plotted along the q_z and q_{xy} axes from the two-dimensional images. As shown in Figure 3(a), the GIXRD images of the PHTBTz-H films display only a diffused first order (100) peak along the q_z axis (out-of-plane), which means that the PHTBTz-H film has a low crystallinity. In contrast, the PHTBTz-C8 film shows stronger out of plane ordering, (h00) with very little arcing. The in-plane $\pi-\pi$ crystal truncation rods, which give rise to the (003) and (010) peaks, are clearly defined and are narrower than in the other samples. This result indicates that edge-on orientation of the PHTBTz-C8 polymer lamellae is achieved on the ODTS treated SiO_2 surface, as is commonly reported for regioregular poly(3-hexylthiophene) (rr-P_3HT).[16] For the PHTBTz-C12 film, out of plane ordering also occurs, but this texture is not as pronounced as in the PHTBTz-C8 film, indicating a weaker nanostructure formation in PHTBTz-C12.

From the high-resolution specular diffraction patterns as shown in Figure 3(d), the lamellar *d*-spacings are evaluated to be 15.5, 17.7, and 21.5 Å for PHTBTz-H, -C8, and -C12, respectively. In the lamellae, generally, the conjugated $\pi-$orbital planes are vertical to the surface plane, forming face-to-face $\pi-\pi$ stacking with crystalline domains somewhat tilted with respect to each other. The lamellar ordering feature for the PHTBTz series is significantly affected by the number of the alkyl side chains and their position.[4,11,13] The PHTBTz-H polymer terminated with H at the R_1 position shows only one order lamellar peak, while the PHTBTz-C8 and -C12, which have the alkyl side chains at both the R_1 and R_2 positions, provided at least four ordered peaks with little arcing, indicating more highly ordered lamellar structures. This may lead us to suspect that the alkyl chains introduced at the R_2 position are more effective at interlocking adjacent polymer chains, yielding highly ordered structures. On the other hand, the length of alkyl side chains may also influence the degree of $\pi-\pi$ stack.[11,17] As mentioned in the above paragraph, the GIXRD images of PHTBTz-C12 that has four additional methylene units in the side chain display more diffuse spots, thus the PHTBTz-C12 might have less crystalline ordering compared to PHTBTz-C8. These differences are more clearly observable in the high-resolution grazing incident diffraction patterns as shown in Figure 3(e). The (003) peaks in the smaller angle region can be assigned to the scattering from the alkyl side chains and the (010) peaks in the higher angle region may be interpreted as the $\pi-\pi$ stacking distance. The (003) peak of PHTBTz-C8 is less intense than that of PHTBTz-C12, since the longer alkyl chains have more electrons to scatter and thus results in a stronger peak. However, the (010) peak of the PHTBTz-C8 is more intense than that of -C12, indicating that the degree of $\pi-\pi$ stacking is higher in the in-plane direction for PHTBTz-C8 containing the shorter alkyl side chains. For the above reasons, it may be inferred that the interlocking of neighboring polymer chains is impeded by steric hindrance due to longer alkyl side chains in PHTBTz-C12.[11,13]

Figure 4 shows tapping-mode atomic force microscopy (AFM) images of PHTBTz-H, -C8, and -C12 thin films prepared on ODTS-treated SiO_2 substrates. While no clear crystalline surface morphology is observed in the PHTBTz-H film, the PHTBTz-C8 film has a highly compact nanofibrillar morphology, which arises from the self-assembly of PHTBTz-C8 chains oriented perpendicular to the substrate in the highly crystalline phase, as is consistent with well-ordered structures confirmed by GIXRD measurements. On the other hand, the PHTBTz-C12 film exhibits a nodule-like nanostructure with some nanofibers, resulting from the misorientation of PHTBTz-C12 chains. The nodule formation in the PHTBTz-C12 film may be attributed to a relatively lower degree of molecular ordering.[18,19]

Side Chain Dependent Field-Effect Mobility. In order to evaluate the electrical properties of the synthesized PHTBTz polymers, coplanar structured OFETs were fabricated using spin-coating and inkjet printing. First, for the spin-coated film based OFET devices, heavily doped silicon was used as the gate

dx.doi.org/10.1021/cm400592b | *Chem. Mater.* 2013, 25, 1927−1934

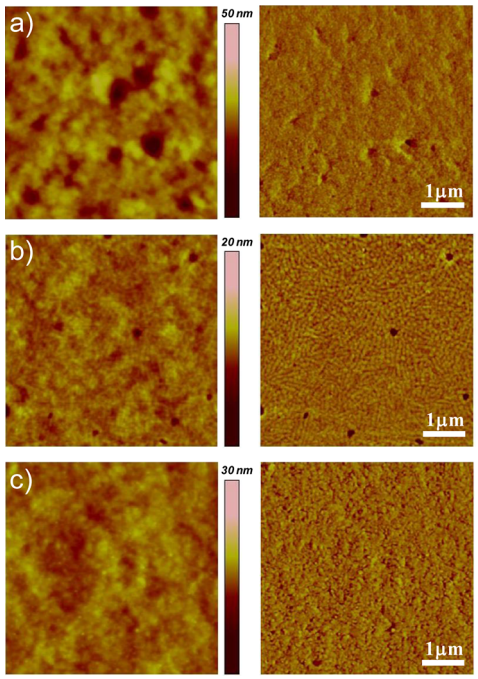

Figure 4. Tapping mode AFM images of (a) PHTBTz-H, (b) PHTBTz-C8, and (c) PHTBTz-C12. The left panel images are the topographic images, and the right panel images are the phase images.

electrode, with ODTS-treated 300 nm-thick layer of thermally grown SiO_2 as the gate dielectric layer. Gold was thermally evaporated and patterned with shadow masks, defining a channel length (L) of 100 μm and a channel width (W) of 1000 μm. Figure 5 shows the transfer curves (upper panel) obtained in the linear (V_{DS} = −10 V) and the saturation (V_{DS} = −40 V) regimes, and the output curves were measured at V_G = 10 V ∼ −50 V with −10 V increments. The field-effect mobility extracted from $|I_{DS}|^{1/2}$ versus V_G curves were 0.002, 0.160, and 0.120 $cm^2\ V^{-1}\ s^{-1}$ for PHTBTz-H, PHTBTz-C8, and PHTBTz-C12, respectively.

The transfer curves in Figure 6 were obtained from the inkjet-printed PHTBTz's based OFETs. In order to fabricate the inkjet-printed OFET device set, as done for the spin-coated film based OFETs, ODTS surface treatment was performed onto the SiO_2 gate dielectric with photolithographically patterned gold source/drain electrodes, before printing the active layers with PHTBTz's based inks. For the inkjet-printed OFETs, the PHTBTz-C8 based device exhibits the best performance with a maximum current of about 1.8 μA, at a gate bias (V_G) and drain bias (V_{DS}) of −40 V each, while a maximum current of only 100 nA is obtained from the

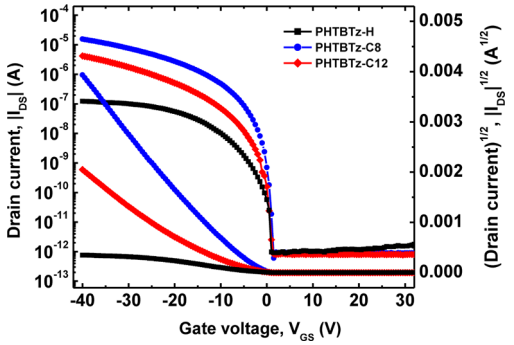

Figure 6. The transfer characteristics of the OFETs based on the PHTBTz series polymers, fabricated by inkjet-printing.

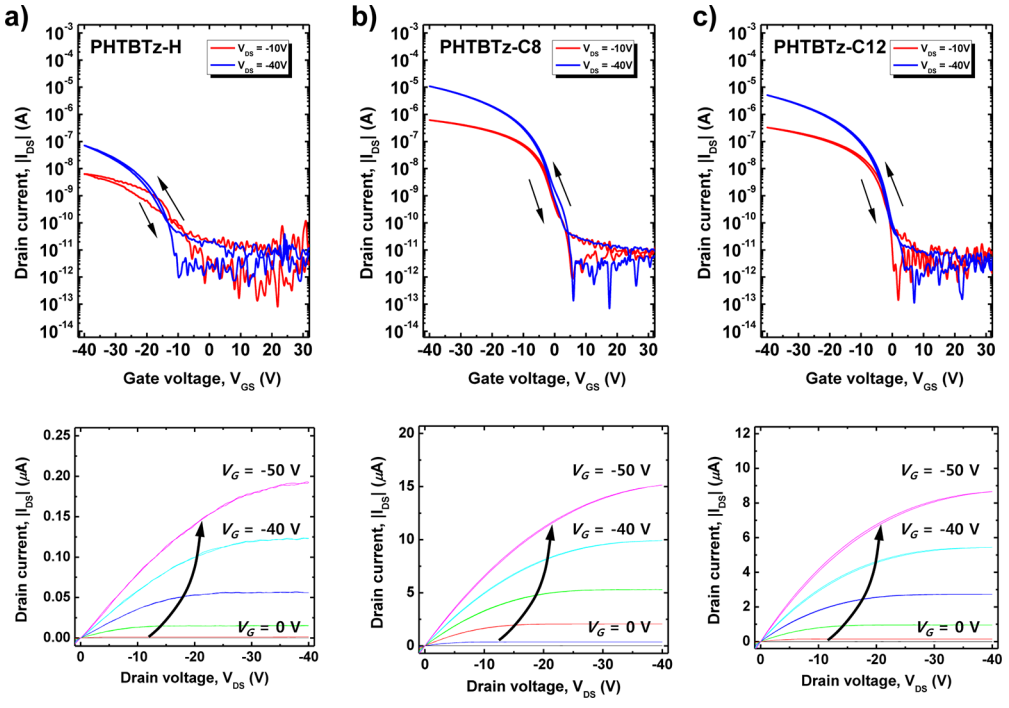

Figure 5. The electrical properties of the spin-coated film based OFETs of PHTBTz-H (a), PHTBTz-C8 (b), and PHTBTz-C12 (c). The transfer curves (upper panel) were obtained from the linear (V_{DS} = −10 V) and the saturation regimes (V_{DS} = −40 V) and the output curves were measured at V_G = 10 V ∼ −50 V with −10 V steps. The estimated field-effect mobility from the slopes of V_{GS}-$|I_D|^{1/2}$ were 0.002, 0.160, and 0.120 $cm^2\ V^{-1}\ s^{-1}$ for PHTBTz-H, PHTBTz-C8, and PHTBTz-C12, respectively.

dx.doi.org/10.1021/cm400592b | *Chem. Mater.* 2013, 25, 1927−1934

Table 2. Device Performance Parameters and Extracted DOS Parameters of the Inkjet-Printed OFETs Based on the PHTBTz Series Polymer Semiconductors

				extracted parameter			
	mobility [$cm^2\ V^{-1}\ s^{-1}$]	ON/OFF ratio	S.S [V/dec.]	N_{TD} [$cm^{-3}\ eV^{-1}$]	kT_{TD} [eV]	N_{DD} [$cm^{-3}\ eV^{-1}$]	kT_{DD} [eV]
PHTBTz-H	0.002	$>10^5$	1.70	1.2×10^{21}	0.06	3.0×10^{19}	0.30
PHTBTz-C8	0.250	$>10^7$	1.05	2.0×10^{20}	0.018	1.0×10^{17}	0.50
PHTBTz-C12	0.097	$>10^6$	1.31	9.0×10^{20}	0.03	1.0×10^{19}	0.21

PHTBTz-H based OFETs. Field-effect mobilities and the device performance parameters extracted from the inkjet-printed PHTBTz series OFETs are summarized in Table 2. The mobility values of the OFETs fabricated by spin-coating and inkjet-printing both suggest that the performance of PHTBTz semiconducting copolymer OFETs is also influenced by the position and length of side chains attached to the backbone, which is consistent with the GIXRD results in that the crystallinity of the PHTBTz series is significantly affected by the number of the alkyl side chains and their positions. A straightforward correlation between device performance and alkyl side chains can be established by considering the crystallinity of the polymer semiconductor. The presence of well-ordered molecules should favor electrical charge transport because the overlap of π−orbitals between conjugated rings increases.[20] Moreover, besides the influence of the π−π stacking, the current in the channel is affected by various traps in the polymer semiconductor film, which can be generated by the loosely packed π−π stacking or mismatched crystalline domains. The free charge carriers can easily move only after filling the trap sites, thus OFETs with an already well-ordered crystalline channel layer can generate enhanced drain currents without loss from trap-related defects.[19,20] This is further supported by the ensuing sub-bandgap density-of-states (DOS) studies of the PHTBTz-based polymer semiconductor films, by applying multiple-frequency capacitance−voltage (MF-CV) spectroscopy on the OFETs.[21]

Influence of Side Chain on Trap Density of States. For a quantitative study of the PHTBTz-based semiconducting copolymers' crystalline quality, we performed MF-CV spectroscopy on the inkjet-printed FETs. Figure 7 shows the trap DOS profiles obtained by the MF-CV spectroscopy (symbols) (details about the measurements are specified in the Supporting Information) and the corresponding exponential DOS model (lines). The DOS model near the valence band maximum (E_V) level [$g(E)$] is described by the superposition of exponential tail states [$g_{TD}(E)$] and exponential deep states [$g_{DD}(E)$] as follows

$$g(E) = g_{DD}(E) + g_{TD}(E)$$
$$= N_{DD} \times \exp\left(\frac{E_V - E}{kT_{DD}}\right) + N_{TD} \times \exp\left(\frac{E_V - E}{kT_{TD}}\right) [eV^{-2}\ cm^{-3}]$$

where N_{DD} is the density of deep states, kT_{DD} is the characteristic energy of deep states, N_{TD} is the density of tail states, and kT_{TD} is the characteristic energy of tail states.[22,23] The DOS model parameters are also summarized in Table 2. Among three kinds of the PHTBTz series, the OFET with the highest mobility (PHTBTz-C8) clearly shows the lowest value of N_{TD} and vice versa. Our findings are theoretically reasonable because as $g(E)$ (i.e., N_{TD}) increases, larger amounts of holes should be expended to fill the traps before the Fermi-energy level approaches E_V.[24,25] Such a loss is followed by degradation in the field-effect mobility at a fixed bias condition. More noticeably, the PHTBTz series-dependence of $g(E)$ is consistent with the aforementioned GIXRD results, because the OFET with a semiconductor of superior crystallinity exhibits the lowest value of N_{TD}. Furthermore, it is worthwhile to note that the N_{TD} value of our PHTBTz-C8 OFETs, 2.0×10^{20} $cm^{-3}\ eV^{-1}$, is even lower than that of pentacene based OFETs calculated by Fortunato et al., which is approximately 1.1×10^{21} $cm^{-3}\ eV^{-1}$.[25] This means that the crystallinity of our PHTBTz-C8 films is superior compared with those reported in former publications by other research groups.[26,27]

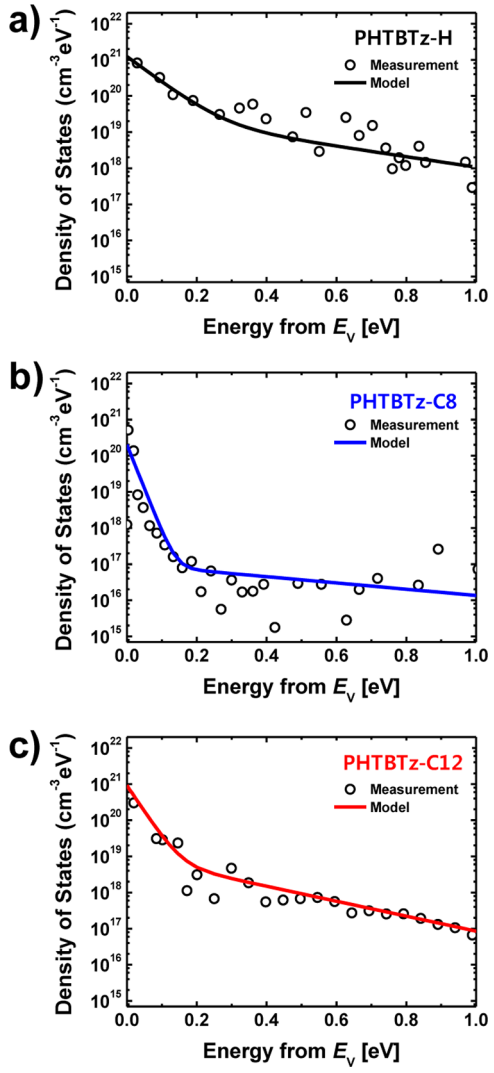

Figure 7. The trap DOS profiles of (a) PHTBTz-H, (b) PHTBTz-C8, and (c) PHTBTz-C12 obtained by MF-CV spectroscopy.

dx.doi.org/10.1021/cm400592b | Chem. Mater. 2013, 25, 1927−1934

CONCLUSION

The results presented here established a critical relationship between the crystallinity of PHTBTz based semiconducting copolymer films and the alkyl side chain's number, position, and length. Furthermore, the extracted trap DOS in the OFETs employing the semiconducting copolymer films as an active layer allowed a quantitative interpretation of the copolymer film crystallinity. Such a relationship between the film microstructure and trap DOS in the OFETs were explained in terms of several competing effects between numbers, positions, and lengths of the alkyl side chain for the efficient $\pi-\pi$ stacking. Additionally, an optimization in the number, position, and length of the alkyl side chains resulted in the synthesis of highly ordered crystalline polymer semiconductor films, at a relatively low annealing temperature of 160 °C. The best performance of the PHTBTz series based OFETs was obtained from the one that exhibited the lowest bulk trap density of $\sim 2.0 \times 10^{20}$ cm^{-3} eV^{-1} with a reasonably high hole mobility of ~ 0.25 cm^2 V^{-1} s^{-1}.

ASSOCIATED CONTENT

Supporting Information

DOS extraction by Multi-frequency Capacitance−Voltage (MF-CV) spectroscopy. This material is available free of charge via the Internet at http://pubs.acs.org.

AUTHOR INFORMATION

Corresponding Author

*E-mail: banglin@samsung.com (B.-L.L.), drlife@kookmin.ac.kr (D.H.K.).

Author Contributions

‡These authors contributed equally.

Notes

The authors declare no competing financial interest.

ACKNOWLEDGMENTS

This work was mainly supported by the Global Leading Technology Program of the Office of Strategic R&D Planning (OSP) funded by the Korean government (MKE) (No. 10042537) and partially supported by the National Research Foundation (NRF) grant funded by MEST (No. 2012-0000147). We gratefully acknowledge helpful technical support of atomic force microscopy by Ms. Y. Kwon in the AE group at Samsung Advanced Institute of Technology, and we also thank Prof. Zhenan Bao and her colleagues at the Stanford University for helpful technical support of synchrotron X-ray diffraction.

ABBREVIATIONS

PHTBTz-H: poly (didodeocylhexathiophene-alt-didodecylbithiazole); PHTBTz-C8: poly(tetryloctylhexathiophene-alt-dioctylbithiazole); PHTBTz-C12: poly(tetryldodecyl-hexathiophene-alt-didodecylbithiazole)

REFERENCES

(1) Chabinyc, M. L.; Salleo, A. *Chem. Mater.* **2006**, *16*, 4509.
(2) Burns, S. E.; Cain, P.; Mills, J.; Wang, J.; Sirringhaus, H. *MRS Bull.* **2003**, *28*, 802.
(3) McCullough, R. D. *Adv. Mater.* **1998**, *10*, 93.
(4) McCulloch, I.; Heeney, M.; Bailey, C.; Genevicius, K.; Macdonald, I.; Shkunov, M.; Sparrowe, D.; Tierney, S.; Wagner, R.; Zhang, W.; Chabinyc, M. L.; Kline, R. J.; McGehee, M. D.; Toney, M. F. *Nat. Mater.* **2006**, *5*, 328.
(5) Yan, H.; Chen, Z. H.; Zheng, Y.; Newman, C.; Quinn, J. R.; Dotz, F.; Kastler, M.; Facchetti, A. *Nature* **2009**, *457*, 679.
(6) Dimitrakopoulos, C. D.; Malenfant, P. R. L. *Adv. Mater.* **2002**, *14*, 99.
(7) Guo, X.; Ortiz, R. P.; Zheng, Y.; Hu, Y.; Noh, Y.-Y.; Baeg, K.-J.; Facchetti, A.; Marks, T. J. *J. Am. Chem. Soc.* **2011**, *133*, 1405.
(8) Allard, S.; Forster, M.; Souharce, B.; Thiem, H.; Scherf, U. *Angew. Chem., Int. Ed.* **2008**, *47*, 4070.
(9) Lee, B.-L.; Han, K.-M.; Lee, E.-K.; Kang, I.-N.; Kim, D. H.; Lee, S. *Synth. Met.* **2009**, *159*, 132.
(10) Kim, D. H.; Lee, B.-L.; Moon, H.; Kang, H. M.; Jeong, E. J.; Park, J.-I.; Han, K.-M.; Lee, S.; Yoo, B. W.; Koo, B.; Kim, J.-Y.; Lee, W. H.; Cho, K.; Becerril, H. A.; Bao, Z. *J. Am. Chem. Soc.* **2009**, *131*, 6124.
(11) Osaka, I.; Zhang, R.; Suave, G.; Smilgies, D.-M.; Kowalewski, T.; McCullough, R. D. *J. Am. Chem. Soc.* **2009**, *131*, 2521.
(12) Guo, X.; Quinn, J.; Chen, Z.; Usta, H.; Zheng, Y.; Xia, Y.; Hennek, J. W.; Ortiz, R. P.; Marks, T. J.; Facchetti, A. *J. Am. Chem. Soc.* **2013**, *135*, 1986.
(13) Ong, B. S.; Wu, Y.; Liu, P. *J. Am. Chem. Soc.* **2004**, *126*, 3378.
(14) Chochos, C. L.; Choulis, S. A. *Prog. Polym. Sci.* **2011**, *36*, 1326.
(15) Osaka, I.; Suave, G.; Zhang, R.; Kowalewski, T.; McCullough, R. D. *Adv. Mater.* **2007**, *131*, 2521.
(16) Sirringhaus, H.; Brown, P. J.; Friend, R. H.; Nielsen, M. M.; Bechgaard, K.; Langeveld-Voss, B. M. W.; Spiering, A. J. H.; Janssen, R. A.; Meijer, E. W.; Herwig, P.; de Leeuw, D. M. *Nature* **1999**, *401*, 685.
(17) Suave, G. A.; Javier, E.; Zhang, R.; Liu, J.; Sydlik, S. A.; Kowalewski, T.; McCullough, R. D. *J. Mater. Chem.* **2010**, *20*, 3195.
(18) Zen, A.; Pflaum, J.; Hirschmann, S.; Zhuang, W.; Jaiser1, F.; Asawapirom, U.; Rabe, J. P.; Scherf, U.; Neher, D. *Adv. Funct. Mater.* **2004**, *14*, 757.
(19) Ong, B. S.; Wu, Y.; Liu, P.; Gardner, S. *Adv. Mater.* **2005**, *9*, 1141.
(20) Sirringhaus, H. *Adv. Mater.* **2005**, *17*, 2411.
(21) Jang, J.; Kim, J.; Bae, M.; Kim, D. M.; Kim, D. H.; Lee, J.; Lee, B.-L.; Koo, B.; Jin, Y. W. *Appl. Phys. Lett.* **2012**, *100*, 133506.
(22) Stallinga, P. *Adv. Mater.* **2011**, *23*, 3356.
(23) Shur, M.; Hack, M. *J. Appl. Phys.* **1984**, *55*, 3831.
(24) Street, R. A.; Song, K. W.; Northrup, J. E.; Cowan, S. *Phys. Rev. B* **2011**, *83*, 165207.
(25) Dacuna, J.; Salleo, A. *Phys. Rev. B* **2011**, *84*, 195209.
(26) Angelis, F.; De Cipolloni, S.; Mariucci, L.; Fortunato, G. *Appl. Phys. Lett.* **2006**, *88*, 193508.
(27) Kalb, W. L.; Batlogg, B. *Phys. Rev. B* **2010**, *81*, 035327.